Rapid Communications

# Two-neutron knockout as a probe of the composition of states in $^{22}$Mg, $^{23}$Al, and $^{24}$Si

B. Longfellow,[1,2] A. Gade,[1,2] J. A. Tostevin,[3] E. C. Simpson,[4] B. A. Brown,[1,2] A. Magilligan,[1,2] D. Bazin,[1,2] P. C. Bender,[1,*] M. Bowry,[1,†] B. Elman,[1,2] E. Lunderberg,[1,2] D. Rhodes,[1,2] M. Spieker,[1,‡] D. Weisshaar,[1] and S. J. Williams[1,§]

[1]*National Superconducting Cyclotron Laboratory, Michigan State University, East Lansing, Michigan 48824, USA*

[2]*Department of Physics and Astronomy, Michigan State University, East Lansing, Michigan 48824, USA*

[3]*Department of Physics, Faculty of Engineering and Physical Sciences, University of Surrey, Guildford, Surrey GU2 7XH, United Kingdom*

[4]*Department of Nuclear Physics, Research School of Physics, The Australian National University, Canberra Australian Capital Territory 2601, Australia*

(Received 12 November 2019; revised manuscript received 4 January 2020; accepted 26 February 2020; published 12 March 2020)

Simpson and Tostevin proposed that the width and shape of exclusive parallel momentum distributions of the $A-2$ residue in direct two-nucleon knockout reactions carry a measurable sensitivity to the nucleon single-particle configurations and their couplings within the wave functions of exotic nuclei. We report here on the first benchmarks and use of this new spectroscopic tool. Exclusive parallel momentum distributions for states in the neutron-deficient nuclei $^{22}$Mg, $^{23}$Al, and $^{24}$Si populated in such direct two-neutron removal reactions were extracted and compared to predictions combining eikonal reaction theory and shell-model calculations. For the well-known $^{22}$Mg and $^{23}$Al nuclei, measurements and calculations were found to agree, supporting the dependence of the parallel momentum distribution width on the angular momentum composition of the shell-model two-neutron amplitudes. In $^{24}$Si, a level at 3439(9) keV, of relevance for the important $^{23}$Al$(p,\gamma)^{24}$Si astrophysical reaction rate, was confirmed to be the $2_2^+$ state, whereas the $4_1^+$ state, expected to be strongly populated in two-neutron knockout, was not observed. This puzzle is resolved by theoretical considerations of the Thomas-Ehrman shift, which also suggests that a previously reported 3471-keV state in $^{24}$Si is, in fact, the $(0_2^+)$ level with one of the largest experimental mirror-energy shifts ever observed.

DOI: 10.1103/PhysRevC.101.031303

One of the major endeavors in nuclear science is the exploration of the evolution of nuclear structure far beyond the valley of $\beta$ stability. For years, direct one-nucleon knockout reactions from projectiles at intermediate energies have been key tools in successfully tracking changes in single-particle energies and strengths toward the nucleon drip lines [1–3]. More recently, it has been shown that two-proton and two-neutron removal from neutron-rich and neutron-deficient projectiles, respectively, also proceed as direct reactions [4,5].

By combining an eikonal model of the reaction dynamics, that assumes a sudden single-step removal of two nucleons and shell-model calculations of the two-nucleon amplitudes (TNAs), the cross sections for two-nucleon knockout from the parent-nucleus ground state to each of the final states in the daughter nucleus can be calculated [6]. Previous work has shown that the shape of the parallel momentum ($p_\parallel$) distribution of the two-nucleon knockout residues depends strongly on the total angular momentum $I$ of the two removed nucleons, allowing spin values to be assigned to populated final states [7–9]. One step further, it was proposed that since the two-nucleon overlaps contain components with different values of total orbital angular momentum $\vec{L}=\vec{l}_1+\vec{l}_2$, information beyond the $I$ value can be probed. This opens up the possibility to uniquely explore this composition and couplings within the wave functions of rare isotopes [10].

In the present Rapid Communication, this configuration sensitivity of the two-neutron knockout-residue $p_\parallel$ distributions is explored with three *sd*-shell cases where the incoming projectiles each have 12 neutrons: $^9$Be($^{24}$Mg, $^{22}$Mg$+\gamma$)$X$, $^9$Be($^{25}$Al, $^{23}$Al$+\gamma$)$X$, and $^9$Be($^{26}$Si, $^{24}$Si$+\gamma$)$X$. From analysis of the exclusive $p_\parallel$ distributions in two-neutron knockout, $J^\pi$ values are assigned, and the dependence of the width on the $L$ composition of the shell-model TNAs is explored, demonstrating the significant utility of this reaction as a spectroscopic tool.

The low-lying level scheme of $^{22}$Mg is well known [11], allowing comparisons of the widths of $p_\parallel$ distributions for several states of the same spin. In $^{23}$Al, only one excited state decays by $\gamma$-ray emission, a core-coupled $7/2^+$ state at 1616(8) keV [12], facilitating clean extraction of the exclusive $p_\parallel$ distributions for the two bound states.

*Present address: Department of Physics, University of Massachusetts Lowell, Lowell, Massachusetts 01854, USA.

†Present address: University of the West of Scotland, Paisley PA1 2BE, United Kingdom.

‡Present address: Department of Physics, Florida State University, Tallahassee, Florida 32306, USA.

§Present address: Diamond Light Source, Harwell Science and Innovation Campus, Didcot, Oxfordshire OX11 0DE, United Kingdom.

 

Excitation energies and $J^\pi$ values in $^{24}$Si are critical for the $^{23}$Al$(p,\gamma)$ rate, which has significant impact on energy generation in type-I X-ray bursts [13,14]. Energy values differing by several 10 keV were reported originally [5,15], and, only recently, a $d(^{23}\mathrm{Al}, ^{24}\mathrm{Si}+\gamma)n$ measurement resolved the discrepancy and, in addition to states at 1874(3) and 3449(5) keV, suggested a new level at 3471(6) keV to be either the $0_2^+$ state with an extremely large Thomas-Ehrman (TE) shift [16,17] or the $4_1^+$ state [18]. To date, all $J^\pi$ assignments are reported as tentative. In this Rapid Communication, two-neutron knockout is used to assign $J^\pi$ values in this key nucleus for the first time.

The experiment was performed at the National Superconducting Cyclotron Laboratory [19]. A secondary beam including $^{24}$Mg (54.5%), $^{25}$Al (29.5%), and $^{26}$Si (13.5%) was produced by impinging the 150-MeV/u $^{36}$Ar primary beam on a 550-mg/cm$^2$ $^9$Be target at the midacceptance position of the A1900 fragment separator [20]. A 250-mg/cm$^2$ achromatic Al wedge was used for secondary beam purification.

Two-neutron knockout reactions were induced on a 287(3)-mg/cm$^2$ $^9$Be target in front of the S800 spectrograph [21]. The midtarget energies for $^{24}$Mg, $^{25}$Al, and $^{26}$Si were 95, 102, and 109 MeV/u, respectively. Event-by-event identification of the incoming projectiles and outgoing reaction products was performed using plastic timing scintillators and the S800 focal-plane detectors [22]. The particle identification plot for incoming $^{26}$Si is shown in Fig. 1 of Refs. [23,24]. For each event, the $p_\parallel$ of the reaction residue at the target was determined using the magnetic rigidity of the S800 spectrograph and the particle trajectory reconstructed from the position and angle measured on the S800 focal plane. To optimize momentum resolution, the S800 analysis beamline was operated in dispersion-matched mode. The target was surrounded by the high-efficiency 192-element caesium-iodide scintillator array CAESAR [25] to tag populated excited states by their in-flight $\gamma$ decays.

The Doppler-corrected $\gamma$-ray spectrum for $^{22}$Mg produced from two-neutron knockout is shown in Fig. 1(a). The proton separation energy of $^{22}$Mg is 5504.3(4) keV [11]. Although peaks at 894, 1247, 2061, 3155, and 3788 keV are clearly visible, $\gamma$-ray transitions above 4 MeV are not resolved. To determine the energies of possible transitions in this region, data from $^{24}$Mg$(p,t)^{22}$Mg [26,27] and $^{12}$C$(^{12}\mathrm{C}, 2n+\gamma)^{22}$Mg [28], which also result in the net loss of two neutrons, were utilized. In all cases, states at 5452 and 5711 keV, which decay primarily by 4205- and 4464-keV $\gamma$ rays, respectively, were populated. Consequently, transitions at these energies were assumed in the fit. To determine exclusive cross sections, the literature branching ratios of known weak decays from the states clearly observed in this Rapid Communication were also included in the fit [11].

Figure 1(b) shows the Doppler-corrected $\gamma$ rays detected in coincidence with $^{23}$Al from two-neutron knockout. $^{23}$Al has a low proton-decay threshold of 141.0(5) keV [11] and only one $\gamma$-ray transition is visible at 1622(6) keV, in agreement with Ref. [12].

Figure 1(c) displays the Doppler-corrected $\gamma$-ray spectrum for $^9$Be$(^{26}\mathrm{Si}, ^{24}\mathrm{Si}+\gamma)X$. Clear peaks at 1569(7) and 1870(6) keV are visible. From $\gamma\gamma$ coincidences and intensities, the 1569-keV transition feeds the 1870-keV level. The energy for the first excited state agrees within uncertainties with all previous measurements [5,15,18]. The resulting energy of the 3439(9)-keV second-excited level, located just above the proton-emission threshold of 3293(20) keV [11] and of importance for the $^{23}$Al$(p,\gamma)^{24}$Si rate, agrees with the 3441(10)-keV value from Ref. [15].

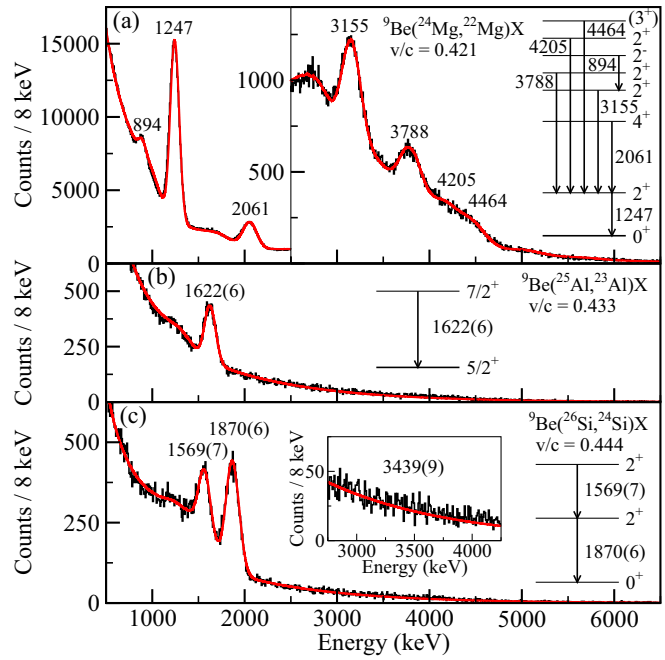


FIG. 1. Doppler-corrected $\gamma$-ray spectra for the reactions (a) $^9$Be$(^{24}\mathrm{Mg}, ^{22}\mathrm{Mg}+\gamma)X$, (b) $^9$Be$(^{25}\mathrm{Al}, ^{23}\mathrm{Al}+\gamma)X$, and (c) $^9$Be$(^{26}\mathrm{Si}, ^{24}\mathrm{Si}+\gamma)X$. The solid red curves are GEANT4 simulations of the observed transitions. Level schemes comprising the most intense transitions are displayed.

The $p_\parallel$ distributions for states in $^{22}$Mg, $^{23}$Al, and $^{24}$Si were obtained by gating on observed $\gamma$-ray transitions. The distributions were background subtracted with significant contributions from Compton-scattered higher-energy transitions accounted for and then corrected for efficiency and feeding according to the level schemes in Fig. 1. The ground-state $p_\parallel$ distributions were obtained by subtracting the distributions of direct feeders from the inclusive $p_\parallel$ distributions. The $p_\parallel$ distributions for the direct feeders in this subtraction were not feeding corrected and, therefore, include contributions from higher-lying levels that do not $\gamma$ decay directly to the ground state.

The theoretical $p_\parallel$ distributions, calculated using eikonal reaction theory and shell-model two-neutron amplitudes from the USD interaction [29,30], were transformed to the laboratory frame and convoluted with a Heaviside function to account for reactions occurring at different depths in the target. To empirically model the low-momentum tails often observed in nucleon knockout, the asymmetric $p_\parallel$ distributions of inelastically scattered projectiles in coincidence with $\gamma$ rays above 500 keV were folded with the calculated distributions

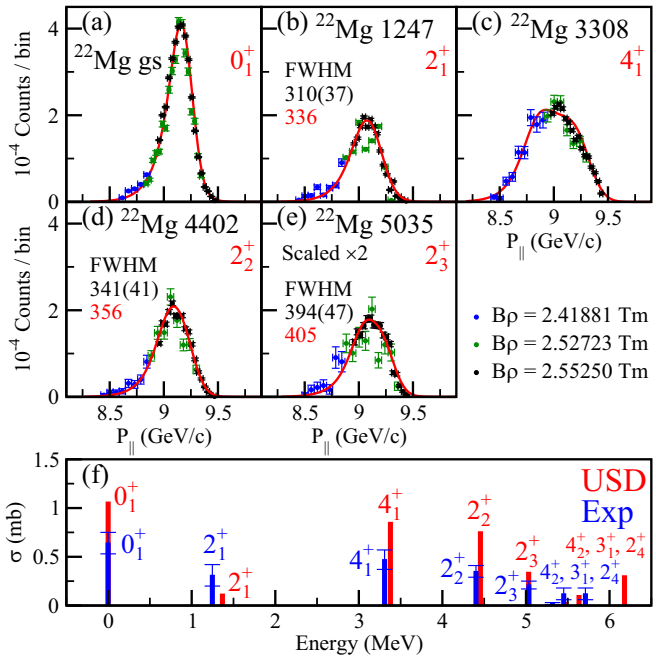


FIG. 2. Parallel momentum ($p_{||}$) distributions for states in $^{22}$Mg populated in two-neutron knockout. The blue, green, and black points correspond to data taken at different magnetic rigidities (B$\rho$) of the S800 spectrograph. The vertical error bars are statistical. The solid red curves are the theoretical $p_{||}$ distributions scaled to best fit the data. The bottom panel compares the measured and calculated cross sections.

following the prescription of Ref. [31]. This approximates the kinematics of the dissipative interactions with the target.

As seen in Fig. 2, the shapes of the theoretical $p_{||}$ distributions are in good agreement with the experimental results for the previously established $0^+_1$, $2^+_1$, $4^+_1$, $2^+_2$, and $2^+_3$ states in $^{22}$Mg. Experimental data were taken at several magnetic rigidity settings of the S800 spectrograph to probe the full $p_{||}$ distributions. Since two neutrons are knocked out from the $0^+$ ground state of $^{24}$Mg, the total angular momentum $I$ of the removed neutrons is the spin $J$ of the populated state in $^{22}$Mg. The spectroscopic power of two-neutron ($2n$) knockout is evident from the $2^+_1$, $2^+_2$, and $2^+_3$ state $p_{||}$ distributions. Although of the same $J^\pi$, the theoretical calculations correctly predict the observed variations in the widths of their $p_{||}$ distributions, the result of different $L$ compositions of their TNAs [10,32]. That the three states are different is evident in Table I where the largest $jj$-coupled TNA for each final state

TABLE I. TNAs calculated in the $jj$, $np$ basis using the USD interaction for the first three $2^+$ states in $^{22}$Mg populated in two-neutron knockout.

| $J^\pi$ | $[1d_{5/2}]^2$ | $[1d_{5/2}, 1d_{3/2}]$ | $[1d_{5/2}, 2s_{1/2}]$ | $[1d_{3/2}]^2$ | $[1d_{3/2}, 2s_{1/2}]$ |
|---|---|---|---|---|---|
| $2^+_1$ | −0.088 | 0.354 | −0.070 | 0.026 | −0.033 |
| $2^+_2$ | −0.756 | 0.222 | −0.219 | −0.044 | 0.221 |
| $2^+_3$ | −0.244 | −0.187 | −0.377 | −0.169 | 0.117 |

involves different $2n$ configurations, $[1d_{5/2}, 1d_{3/2}]$, $[1d_{5/2}]^2$, and $[1d_{5/2}, 2s_{1/2}]$. A full analysis of the $L$ makeup from all TNAs (provided in the Supplemental Material [33]), reveals a significant (narrower) $L = 1$, $2^+_1$ component, that is smaller (relative to $L = 2$) for $2^+_2$, and which is essentially zero for $2^+_3$, in line with the reported $p_{||}$ distributions.

Figure 2(f) shows the experimental partial cross sections extracted for states in $^{22}$Mg compared to the cross sections calculated using the USD TNAs. Previous work on two-nucleon knockout [4–6,34] has found a ratio of approximately 0.5 between experimental and theoretical inclusive cross sections in the *sd* shell. For the $0^+_1$, $4^+_1$, $2^+_2$, and $2^+_3$ states, the partial cross sections are 0.64(11), 0.47(10), 0.35(6), and 0.21(4) mb, giving ratios to the theoretical calculations of 0.60(10), 0.55(12), 0.46(8), and 0.62(11), respectively. Interestingly, the experimental cross section for the $2^+_1$ state is 0.31(11) mb whereas the theoretical prediction is 0.117 mb. This is likely due to incomplete subtraction of feeding from several higher-lying states, including $2^-$ and $3^-$ levels formed in the removal of one neutron each from the $1d_{5/2}$ and $1p_{1/2}$ orbitals. Evidence for their population here is, for example, the 894-keV $\gamma$ ray attributed to the $2^- \rightarrow 2^+_2$ transition in $^{22}$Mg [28]. From the mirror $^{22}$Ne [11], sizable transitions to the $2^+_1$ state, falling into the region of unresolved transitions above 4 MeV, are expected from this $2^-$ state and from a $3^-$ state around 6 MeV. A partial cross section of 0.08(3) mb to the $2^-$ state at 5296 kev was inferred using only the 894-keV transition, but the total possible cross section to all $2^-$ states from removal of one $1d_{5/2}$ and one $1p_{1/2}$ neutron is 1.687 mb. Only a small fraction of this strength is needed to account for the suspected unobserved feeding of the $2^+_1$ state. Unfortunately, the shapes of the calculated $2^-$ and $2^+_1$ $p_{||}$ distributions are too similar to serve as a discriminator.

The inclusive cross section for two-neutron knockout is 2.24(34) mb, excluding the cross section to the $2^-$ state. The theoretical inclusive cross section for *sd*-shell states up to the $2^+_3$ level is 3.572 mb, giving a ratio for experiment to theory of 0.63(10). Although this ratio is slightly above the typical ratio of about 0.5, should some of the cross section to negative-parity states have been misattributed to *sd*-shell states, the ratio would decrease.

The measured and predicted $p_{||}$ distributions for the $5/2^+$ ground and the $7/2^+$ excited state of $^{23}$Al populated from the $^{25}$Al($5/2^+$) ground state are shown in Fig. 3. Knockout to the $5/2^+$ level in $^{23}$Al has contributions from *sd*-shell neutrons coupled to $I = 0$-4 with a predicted dominance of the $I = 0$ component. Knockout to the $7/2^+$ state involves $I = 1$-4 contributions with $I = 4$ larger than $I = 2$ by about a factor of 2. For both, the odd-$I$ TNAs are negligible. The experimental $p_{||}$ distributions reflect this $I$ composition of the shell-model wave function with a narrow $5/2^+$ and a broad $7/2^+$ $p_{||}$ distribution.

The partial cross sections for the $5/2^+$ and $7/2^+$ states are 0.60(8) and 0.09(3) mb, respectively, and the inclusive cross section is 0.69(9) mb. The ratios to the theoretical calculations for the $5/2^+$, $7/2^+$, and inclusive cross sections are 0.55(7), 0.54(18), and 0.55(7). The centroids of the $p_{||}$ distributions

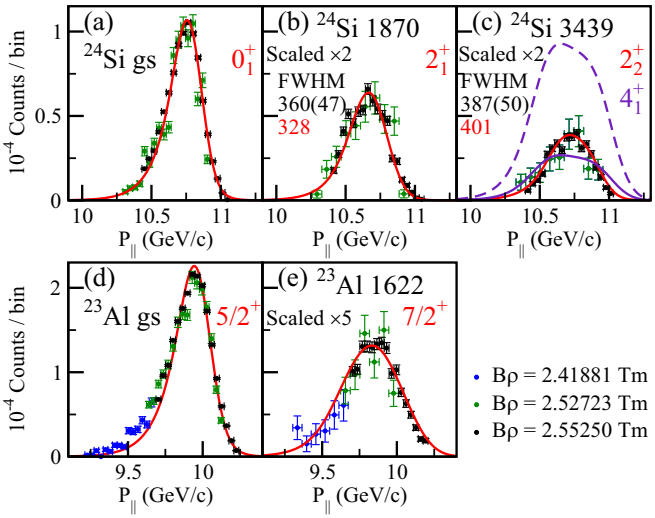


FIG. 3. Parallel momentum ($p_{\parallel}$) distributions for states in $^{23}$Al and $^{24}$Si populated in two-neutron knockout. The blue, green, and black points correspond to data taken at different magnetic rigidities (B$\rho$) of the S800 spectrograph. The vertical error bars are statistical. The solid red and purple curves are the theoretical $p_{\parallel}$ distributions scaled to best fit the data. The dashed purple curve shows the distribution for the $4_1^+$ state in $^{24}$Si assuming the theoretical cross section times 0.5.

for the different final states are slightly shifted with respect to each other as reported in Ref. [9].

Figure 3 shows the measured and calculated $p_{\parallel}$ distributions for levels in $^{24}$Si populated in two-neutron knockout from the $^{26}$Si($0^+$) ground state. The shapes of the predicted distributions for the ground and $2_1^+$ states agree well with the data. Shell-model calculations and comparisons with the mirror nucleus predict close-lying $2_2^+$ and $4_1^+$ levels in $^{24}$Si. As seen in Fig. 3(c), the data for the 3439(9)-keV level support a $J^{\pi}$ assignment of $2_2^+$ rather than $4_1^+$. Since the experimental $p_{\parallel}$ distribution is slightly narrower than the theoretical $2_2^+$ distribution, adding a $4_1^+$ component to the fit does not improve the agreement. The measured widths of the $2_1^+$ and $2_2^+$ $p_{\parallel}$ distributions are consistent with the predicted dominance of $L = 1$ and $L = 2$, respectively, in the decomposition of the TNAs (see Tables III and IV and accompanying text of Ref. [10]). In the mirror $^{24}$Ne, the $2_2^+$ has relative $\gamma$-decay intensities of 100.0(22) to the $2_1^+$ and 11.1(22) to the ground state. From our spectra [see Fig. 1(c)], a ground-state branch of larger than 4% can be excluded.

The partial cross sections for the $0_1^+$, $2_1^+$, and $2_2^+$ states in $^{24}$Si are 0.62(8), 0.17(3), and 0.13(3) mb, giving ratios to theory of 0.48(6), 0.53(9), and 0.40(9). The inclusive cross section is 0.92(10) mb giving a ratio to theory of 0.47(5). These results agree with the cross sections reported in Ref. [5].

In the recent $d(^{23}\mathrm{Al}, ^{24}\mathrm{Si})n$ work, $\gamma$-ray transitions at 1575(3) keV from the ($2_2^+$) level at 3449(5) and 1597(5) keV from the ($4_1^+, 0_2^+$) level at 3471(6) keV were proposed [18]. The results presented here for the 3439(9)-keV state confirm the $2_2^+$ assignment. If a transition at 1597 keV is included in the fit of the $\gamma$-ray spectrum in Fig. 1(c), its intensity is, at most, 7% of the 1570-keV transition, consistent with its nonobservation in Ref. [5]. The knockout calculation predicts a large cross section of 0.935 mb to the $4_1^+$ state as compared to 0.329 mb to the $2_2^+$ state. The dashed purple curve in Fig. 3(c) shows the expected $4_1^+$ $p_{\parallel}$ distribution assuming a cross section of 0.5 times the prediction. If the 3471-keV level is the $4_1^+$ state, then the 1597-keV transition should have been observed here. Conversely, the predicted cross section for the $0_2^+$ state in two-neutron knockout is only 0.005 mb, consistent with the nonobservation of the 1597-keV transition. As noted in Ref. [18], if the 3471-keV level in $^{24}$Si is the $0_2^+$ state, then its energy is 1296 keV below the $0_2^+$ state in $^{24}$Ne.

TABLE II. TE shifts for states in $^{23}$Al and $^{24}$Si. The summed one-proton TE contributions are added to the experimental energies of the mirror states in $^{23}$Ne and $^{24}$Ne [11]. The $C^2S$ and $S'_p = S_p(^AZ) + E_x(^{A-1}Z-1) - E_x(^AZ)$ for the dominant term of the sum are shown. $E_{\mathrm{mirr}} + \mathrm{TE}$ energies are reported relative to the ground state and compared with the measured values of Ref. [11] for $^{23}$Al and Ref. [18] for $^{24}$Si. For the $4^+$ and $0_2^+$ states in $^{24}$Si, $E_{\mathrm{exp}}$ are both reported as 3471 keV for comparison.

| | $J^{\pi}$ | $C^2S$ | $S'_p$ (keV) | TE (keV) | $E_{\mathrm{mirr}}$ (keV) | $E_{\mathrm{mirr}} + \mathrm{TE}$ (keV) | $E_{\mathrm{exp}}$ (keV) |
|---|---|---|---|---|---|---|---|
| $^{23}$Al | $5/2^+$ | 0.003 | 1484 | −1 | 0 | 0 | 0 |
| | $1/2^+$ | 0.704 | −409 | −427 | 1017 | 590 | 550(20) |
| $^{24}$Si | $0^+$ | 0.226 | 3843 | −57 | 0 | 0 | 0 |
| | $2^+$ | 0.191 | 1419 | −84 | 1982 | 1955 | 1874(3) |
| | $2^+$ | 0.500 | −156 | −253 | 3868 | 3672 | 3449(5) |
| | $4^+$ | 0.052 | 3804 | −17 | 3972 | 4011 | 3471(6) |
| | $0^+$ | 1.083 | −118 | −534 | 4767 | 4290 | 3471(6) |

To explore the expected TE shifts for states in $^{24}$Si, proximity to the one-proton threshold of 3293(20) keV [11] was considered. For a state in $^{24}$Si with excitation energy $E_x(^{24}\mathrm{Si})$, the TE shift due to the one-proton separation energy relative to excited states in $^{23}$Al below 4 MeV is as follows:

$$\mathrm{TE}[E_x(^{24}\mathrm{Si})] = \left(\frac{24}{23}\right)^2 \sum_{E_x(^{23}\mathrm{Al})}^{4\ \mathrm{MeV}} C^2S(^{24}\mathrm{Si}\rightarrow{}^{23}\mathrm{Al}) \times \mathrm{TE}_{\mathrm{WS}}[S_p(^{24}\mathrm{Si}) + E_x(^{23}\mathrm{Al}) - E_x(^{24}\mathrm{Si})].$$

Here, $\mathrm{TE}_{\mathrm{WS}}$ is the single-proton TE shift calculated from a Woods-Saxon potential. The factor of $(24/23)^2$ is the center-of-mass correction [35,36]. The spectroscopic factors $C^2S$, are for one-proton $2s_{1/2}$ overlaps as in Ref. [24]. The resulting relative TE shift for each level is added to the measured energy of the $^{24}$Ne mirror state. The results are summarized in Table II together with the TE shift for the $^{23}$Al $1/2^+$ state calculated using the same method, in good agreement with experiment.

The TE shift for the $4^+$ state in $^{24}$Si is minimal, predicting an energy of 4011 keV. If the $4^+$ level is around 4 MeV, then the one- and two-proton decays of the state would dominate, explaining the nonobservation of its $\gamma$ decay in this Rapid Communication. The $0_2^+$ state in $^{24}$Si is shifted down by 477 to 4290 keV. The $2s_{1/2}$ overlap that dominates the TE shift for the $0_2^+$ level is with the $1/2^+$ state in $^{23}$Al, which itself has a large relative TE shift of 426 keV.

The $0_2^+$ state has a large $[2s_{1/2}]^2$ two-proton overlap with the ground state of $^{22}$Mg, and the 3471(6)-keV level in $^{24}$Si is only 37(20) keV above $S_{2p} = 3434(19)$ keV [11]. Other examples of $0^+$ two-proton configurations lying just above the two-proton decay thresholds with large mirror-energy shifts can be found in $^{18}$Ne [11] and $^{14}$O [37]. Also, the unbound $^{26}$O lies only 18 keV above the two-neutron separation energy [38]. If the 3471-keV level in $^{24}$Si is our proposed $0_2^+$, its large TE shift might be connected with its proximity to the two-proton decay threshold. Mirror symmetry is frequently evoked in nuclear astrophysics for the identification and characterization of important levels for capture-reaction networks, e.g., in the *rp* process [39–43]. Isospin-symmetry-breaking effects as large as the TE shift suggested here complicate such analyses significantly and must be considered.

To summarize, the reactions $^9$Be($^{24}$Mg, $^{22}$Mg $+\gamma$)$X$, $^9$Be($^{25}$Al, $^{23}$Al $+\gamma$)$X$, and $^9$Be($^{26}$Si, $^{24}$Si $+\gamma$)$X$ were used to benchmark the sensitivity of theoretical parallel momentum distribution calculations to the components in the shell-model two-neutron overlaps. In $^{22}$Mg and $^{23}$Al, the shapes of the exclusive parallel momentum distributions were in good agreement with theoretical predictions, realizing the high spectroscopic potential of two-nucleon knockout. In $^{24}$Si, the 3439-keV state, important for the proton-capture reaction rate, was confirmed as the $2_2^+$ level. The predicted $4_1^+$ shell-model state in $^{24}$Si, expected to be strongly populated in two-neutron knockout, was not observed. By considering Thomas-Ehrman shifts and proximity to the two-proton separation energy, we propose that the 3471-keV state reported in Ref. [18] is the $(0_2^+)$ rather than the $(4_1^+)$ state. Consequently, the experimental mirror-energy shift for the $(0_2^+)$ level in $^{24}$Si is among the largest ever observed.

This Rapid Communication was supported by the National Science Foundation (NSF) under Grants No. PHY-1102511 and No. PHY-1565546, by the DOE National Nuclear Security Administration through the Nuclear Science and Security Consortium, under Award No. DE-NA0003180, and by the Department of Energy, Office of Nuclear Physics, under Grants No. DE-FG02-08ER41556 and No. DE-SC0020451. J.A.T acknowledges support from the Science and Technology Facilities Council (U.K.) Grant No. ST/L005743/1. B.A.B. acknowledges support from NSF Grant No. PHY-1811855. The authors wish to thank M. Płoszajczak and A. Volya for helpful discussions.

[1] P. G. Hansen and J. A. Tostevin, Annu. Rev. Nucl. Part. Sci. **53**, 219 (2003).
[2] A. Gade and T. Glasmacher, Prog. Part. Nucl. Phys. **60**, 161 (2008).
[3] A. Obertelli, Eur. Phys. J. Plus **131**, 319 (2016).
[4] D. Bazin, B. A. Brown, C. M. Campbell, J. A. Church, D. C. Dinca, J. Enders, A. Gade, T. Glasmacher, P. G. Hansen, W. F. Mueller, H. Olliver, B. C. Perry, B. M. Sherrill, J. R. Terry, and J. A. Tostevin, Phys. Rev. Lett. **91**, 012501 (2003).
[5] K. Yoneda, A. Obertelli, A. Gade, D. Bazin, B. A. Brown, C. M. Campbell, J. M. Cook, P. D. Cottle, A. D. Davies, D.-C. Dinca, T. Glasmacher, P. G. Hansen, T. Hoagland, K. W. Kemper, J.-L. Lecouey, W. F. Mueller, R. R. Reynolds, B. T. Roeder, J. R. Terry, J. A. Tostevin, and H. Zwahlen, Phys. Rev. C **74**, 021303(R) (2006).
[6] J. A. Tostevin and B. A. Brown, Phys. Rev. C **74**, 064604 (2006).
[7] E. C. Simpson, J. A. Tostevin, D. Bazin, B. A. Brown, and A. Gade, Phys. Rev. Lett. **102**, 132502 (2009).
[8] E. C. Simpson, J. A. Tostevin, D. Bazin, and A. Gade, Phys. Rev. C **79**, 064621 (2009).
[9] D. Santiago-Gonzalez, I. Wiedenhöver, V. Abramkina, M. L. Avila, T. Baugher, D. Bazin, B. A. Brown, P. D. Cottle, A. Gade, T. Glasmacher, K. W. Kemper, S. McDaniel, A. Rojas, A. Ratkiewicz, R. Meharchand, E. C. Simpson, J. A. Tostevin, A. Volya, and D. Weisshaar, Phys. Rev. C **83**, 061305(R) (2011).
[10] E. C. Simpson and J. A. Tostevin, Phys. Rev. C **82**, 044616 (2010).
[11] Evaluated Nuclear Structure Data File (ENSDF) [http://www.nndc.bnl.gov/ensdf].
[12] A. Gade, P. Adrich, D. Bazin, M. D. Bowen, B. A. Brown, C. M. Campbell, J. M. Cook, T. Glasmacher, K. Hosier, S. McDaniel, D. McGlinchery, A. Obertelli, L. A. Riley, K. Siwek, J. A. Tostevin, and D. Weisshaar, Phys. Lett. B **666**, 218 (2008).
[13] A. Parikh, J. José, F. Moreno, and C. Iliadis, Astrophys. J., Suppl. Ser. **178**, 110 (2008).
[14] R. H. Cyburt, A. M. Amthor, A. Heger, E. Johnson, L. Keek, Z. Meisel, H. Schatz, and K. Smith, Astrophys. J., Suppl. Ser. **830**, 55 (2016).
[15] H. Schatz, J. Görres, H. Herndl, N. I. Kaloskamis, E. Stech, P. Tischhauser, M. Wiescher, A. Bacher, G. P. A. Berg, T. C. Black, S. Choi, C. C. Foster, K. Jiang, and E. J. Stephenson, Phys. Rev. Lett. **79**, 3845 (1997).
[16] J. B. Ehrman, Phys. Rev. **81**, 412 (1951).
[17] R. G. Thomas, Phys. Rev. **88**, 1109 (1952).
[18] C. Wolf, C. Langer, F. Montes, J. Pereira, W.-J. Ong, T. Poxon-Pearson, S. Ahn, S. Ayoub, T. Baumann, D. Bazin, P. C. Bender, B. A. Brown, J. Browne, H. Crawford, R. H. Cyburt, E. Deleeuw, B. Elman, S. Fiebiger, A. Gade, P. Gastis, S. Lipschutz, B. Longfellow, Z. Meisel, F. M. Nunes, G. Perdikakis, R. Reifarth, W. A. Richter, H. Schatz, K. Schmidt, J. Schmitt, C. Sullivan, R. Titus, D. Weisshaar, P. J. Woods, J. C. Zamora, and R. G. T. Zegers, Phys. Rev. Lett. **122**, 232701 (2019).
[19] A. Gade and B. M. Sherrill, Phys. Scr. **91**, 053003 (2016).
[20] D. J. Morrissey, B. M. Sherrill, M. Steiner, and I. Wiedenhoever, Nucl. Instrum. Methods Phys. Res., Sect. B **204**, 90 (2003).
[21] D. Bazin, J. A. Caggiano, B. M. Sherrill, J. Yurkon, and A. Zeller, Nucl. Instrum. Methods Phys. Res., Sect. B **204**, 629 (2003).
[22] J. Yurkon, D. Bazin, W. Benenson, D. J. Morrissey, B. M. Sherrill, D. Swan, and R. Swanson, Nucl. Instrum. Methods Phys. Res., Sect. A **422**, 291 (1999).

[23] B. Longfellow, A. Gade, B. A. Brown, W. A. Richter, D. Bazin, P. C. Bender, M. Bowry, B. Elman, E. Lunderberg, D. Weisshaar, and S. J. Williams, Phys. Rev. C **97**, 054307 (2018).

[24] B. Longfellow, A. Gade, B. A. Brown, D. Bazin, P. C. Bender, M. Bowry, P. D. Cottle, B. Elman, E. Lunderberg, A. Magilligan, M. Spieker, D. Weisshaar, and S. J. Williams, Phys. Rev. C **99**, 064330 (2019).

[25] D. Weisshaar, A. Gade, T. Glasmacher, G. F. Grinyer, D. Bazin, P. Adrich, T. Baugher, J. M. Cook, C. Aa. Diget, S. McDaniel, A. Ratkiewicz, K. P. Siwek, and K. A. Walsh, Nucl. Instrum. Methods Phys. Res., Sect. A **624**, 615 (2010).

[26] K. Y. Chae, D. W. Bardayan, J. C. Blackmon, K. A. Chipps, R. Hatarik, K. L. Jones, R. L. Kozub, J. F. Liang, C. Matei, B. H. Moazen, C. D. Nesaraja, P. D. O'Malley, S. D. Pain, S. T. Pittman, and M. S. Smith, Phys. Rev. C **79**, 055804 (2009).

[27] A. Matic, A. M. van den Berg, M. N. Harakeh, H. J. Wörtche, G. P. A. Berg, M. Couder, J. L. Fisker, J. Görres, P. LeBlanc, S. O'Brien, M. Wiescher, K. Fujita, K. Hatanaka, Y. Sakemi, Y. Shimizu, Y. Tameshige, A. Tamii, M. Yosoi, T. Adachi, Y. Fujita, Y. Shimbara, H. Fujita, T. Wakasa, P. O. Hess, B. A. Brown, and H. Schatz, Phys. Rev. C **80**, 055804 (2009).

[28] D. Seweryniak, P. J. Woods, M. P. Carpenter, T. Davinson, R. V. F. Janssens, D. G. Jenkins, T. Lauritsen, C. J. Lister, C. Ruiz, J. Shergur, S. Sinha, and A. Woehr, Phys. Rev. Lett. **94**, 032501 (2005).

[29] B. H. Wildenthal, Prog. Part. Nucl. Phys. **11**, 5 (1984).

[30] B. A. Brown and B. H. Wildenthal, Annu. Rev. Nucl. Part. Sci. **38**, 29 (1988).

[31] S. R. Stroberg, A. Gade, J. A. Tostevin, V. M. Bader, T. Baugher, D. Bazin, J. S. Berryman, B. A. Brown, C. M. Campbell, K. W. Kemper, C. Langer, E. Lunderberg, A. Lemasson, S. Noji, F. Recchia, C. Walz, D. Weisshaar, and S. J. Williams, Phys. Rev. C **90**, 034301 (2014).

[32] J. A. Tostevin, G. Podolyák, B. A. Brown, and P. G. Hansen, Phys. Rev. C **70**, 064602 (2004).

[33] See Supplemental Material at http://link.aps.org/supplemental/10.1103/PhysRevC.101.031303 for further details on the *LS*-decomposed TNAs.

[34] K. Wimmer, D. Bazin, A. Gade, J. A. Tostevin, T. Baugher, Z. Chajecki, D. Coupland, M. A. Famiano, T. K. Ghosh, G. F. Grinyer, R. Hodges, M. E. Howard, M. Kilburn, W. G. Lynch, B. Manning, K. Meierbachtol, P. Quarterman, A. Ratkiewicz, A. Sanetullaev, S. R. Stroberg, M. B. Tsang, D. Weisshaar, J. Winkelbauer, R. Winkler, and M. Youngs, Phys. Rev. C **85**, 051603(R) (2012).

[35] J. B. French and M. H. Macfarlane, Nucl. Phys. **26**, 168 (1961).

[36] A. E. L. Dieperink and T. de Forest, Phys. Rev. C **10**, 543 (1974).

[37] R. J. Charity, K. W. Brown, J. Okołowicz, M. Płoszajczak, J. M. Elson, W. Reviol, L. G. Sobotka, W. W. Buhro, Z. Chajecki, W. G. Lynch, J. Manfredi, R. Shane, R. H. Showalter, M. B. Tsang, D. Weisshaar, J. R. Winkelbauer, S. Bedoor, and A. H. Wuosmaa, Phys. Rev. C **100**, 064305 (2019).

[38] Y. Kondo, T. Nakamura, R. Tanaka, R. Minakata, S. Ogoshi, N. A. Orr, N. L. Achouri, T. Aumann, H. Baba, F. Delaunay, P. Doornenbal, N. Fukuda, J. Gibelin, J. W. Hwang, N. Inabe, T. Isobe, D. Kameda, D. Kanno, S. Kim, N. Kobayashi, T. Kobayashi, T. Kubo, S. Leblond, J. Lee, F. M. Marque's, T. Motobayashi, D. Murai, T. Murakami, K. Muto, T. Nakashima, N. Nakatsuka, A. Navin, S. Nishi, H. Otsu, H. Sato, Y. Satou, Y. Shimizu, H. Suzuki, K. Takahashi, H. Takeda, S. Takeuchi, Y. Togano, A. G. Tuff, M. Vandebrouck, and K. Yoneda, Phys. Rev. Lett. **116**, 102503 (2016).

[39] D. Rodríguez, V. S. Kolhinen, G. Audi, J. Äystö, D. Beck, K. Blaum, G. Bollen, F. Herfurth, A. Jokinen, A. Kellerbauer, H.-J. Kluge, M. Oinonen, H. Schatz, E. Sauvan, and S. Schwarz, Phys. Rev. Lett. **93**, 161104 (2004).

[40] A. M. Rogers, M. A. Famiano, W. G. Lynch, M. S. Wallace, F. Amorini, D. Bazin, R. J. Charity, F. Delaunay, R. T. de Souza, J. Elson, A. Gade, D. Galaviz, M.-J. van Goethem, S. Hudan, J. Lee, S. Lobastov, S. Lukyanov, M. Matoš, M. Mocko, H. Schatz, D. Shapira, L. G. Sobotka, M. B. Tsang, and G. Verde, Phys. Rev. Lett. **106**, 252503 (2011).

[41] C. Langer, F. Montes, A. Aprahamian, D. W. Bardayan, D. Bazin, B. A. Brown, J. Browne, H. Crawford, R. H. Cyburt, C. Domingo-Pardo, A. Gade, S. George, P. Hosmer, L. Keek, A. Kontos, I-Y. Lee, A. Lemasson, E. Lunderberg, Y. Maeda, M. Matos, Z. Meisel, S. Noji, F. M. Nunes, A. Nystrom, G. Perdikakis, J. Pereira, S. J. Quinn, F. Recchia, H. Schatz, M. Scott, K. Siegl, A. Simon, M. Smith, A. Spyrou, J. Stevens, S. R. Stroberg, D. Weisshaar, J. Wheeler, K. Wimmer, and R. G. T. Zegers, Phys. Rev. Lett. **113**, 032502 (2014).

[42] V. Margerin, G. Lotay, P. J. Woods, M. Aliotta, G. Christian, B. Davids, T. Davinson, D. T. Doherty, J. Fallis, D. Howell, O. S. Kirsebom, D. J. Mountford, A. Rojas, C. Ruiz, and J. A. Tostevin, Phys. Rev. Lett. **115**, 062701 (2015).

[43] H. Suzuki, L. Sinclair, P.-A. Söderström, G. Lorusso, P. Davies, L. S. Ferreira, E. Maglione, R. Wadsworth, J. Wu, Z. Y. Xu, S. Nishimura, P. Doornenbal, D. S. Ahn, F. Browne, N. Fukuda, N. Inabe, T. Kubo, D. Lubos, Z. Patel, S. Rice, Y. Shimizu, H. Takeda, H. Baba, A. Estrade, Y. Fang, J. Henderson, T. Isobe, D. Jenkins, S. Kubono, Z. Li, I. Nishizuka, H. Sakurai, P. Schury, T. Sumikama, H. Watanabe, and V. Werner, Phys. Rev. Lett. **119**, 192503 (2017).